Available online at www.sciencedirect.com
SCIENCE DIRECT®
International Journal of Thermal Sciences 42 (2003) 1029–1045
International Journal of Thermal Sciences
www.elsevier.com/locate/ijts

An integrated pulse tube refrigeration device with micro exchangers: design and experiments

Philippe Nika [a,c,*], Yannick Bailly [a,c], Jean Claude Jeannot [b,c], Michel De Labachelerie [b,c]

[a] *Centre de recherche sur les écoulements, surfaces et transferts (CREST)/UMR CNRS 6000 – parc technologique, 2, avenue Jean Moulin, 90000 Belfort, France*

[b] *Laboratoire de physique et de métrologie des oscillateurs (LPMO), France*

[c] *Institut des microtechniques de Franche-Comté, 32, avenue de l'observatoire, 25044 Besançon, France*

Received 18 June 2002; accepted 7 March 2003

Abstract

The cooling of electronic components is of great interest to improve their capabilities, especially for CMOS components. The purpose of this paper is to present the principle and the design of a micro cooler dedicated to such application. The originality of the approach concerns both the use of a thermodynamic system and the use of a micro-fabrication technology entirely compatible with the small scale of the component. The cooling function is assumed by a pulsed gas in a small canal (pulse tube) made of glass and of silicon. Specific micro heat exchangers, also made of silicon, have been designed from the results of a study concerning both the pressure drop and the transitory thermal response. The actual micro-cooler performances are estimated in an experimental way by means of temperature and pressure measurements.

Keywords: Micro-coolers; Micro heat exchangers; Regenerator; Silicon technology; Design; Experiments

1. Introduction

In numerous electronic devices the temperature appears to be an important parameter that limits components capabilities so an important request for specific miniature cooling systems exists nowadays. In most applications the cooling function is assumed by a simple ventilation of the component or of the whole electronic card but despite many improvements of these techniques, they do not operate in all cases and they are limited by ambient temperature. Other passive methods like microchannel heat sinks [1] or Miniature Heat Pipes (MHP) [2] have received a great attention and a good level of development has been reached in both for the theory and the applications. High power density with heat flux of a few 100 $W \cdot cm^{-2}$ have been reached with microscopic flow channels in such devices. However, these systems generally use an evaporating liquid that needs to be recycled after evaporation and in case of imperfect sealing, an electrical risk may damage the electronic component to be cooled. In MHP system, in order to limit the pressure level while conserving acceptable performances, the fluid can be acetone, methanol, ethanol and water and the temperature of electronic applications is in the range from 0 °C to 100 °C and never in the cryogenic range. In addition MPH performances depend mainly of the inclination of the tube with respect to the gravity. In fact when lower temperatures are required an alternative solution based on a specific active cooling device is often to be created. Different solutions have been proposed already such thermoelectric coolers or Stirling and Gifford Mac-Mahon refrigerators. In fact, a good cooler dedicated to electronic components may generate neither mechanical vibrations nor electrical perturbations; it may also have a low electrical consumption and may be relatively small regarding the component to be cooled. Thereby, the Pulse Tube Refrigerator (PTR) seems to answer these requirements correctly: no moving mechanical part are used in this kind of device, especially near the cold zone. This means that mechanical vibrations are avoided (which cannot be reached with the Stirling refrigerator). Moreover, the problem of dynamic airtightness due to mechanical movements is very critical at small scale and limits the miniaturization of classical Stirling refrigerator dramatically: again, the PTR technology allows to imagine a high level of miniaturization to reach a cooler which dimensions are similar

* Corresponding author.
E-mail address: philippe.nika@univ-fcomte.fr (P. Nika).

1290-0729/$ – see front matter
doi:10.1016/S1290-0729(03)00081-4

Nomenclature

a	thermal diffusivity	$m^2 \cdot s^{-1}$
a, b, c	constants Eq. (12)	
B, B_0, B_1, B_2, B_3	parameters Eq. (A.3)	
c	thermal capacity	$J \cdot kg^{-1} \cdot K^{-1}$
C_1, C_2, C_3	constants Eq. (24)	
C'_f	pressure drop coefficient	
D, d	diameter	m
disp	displacement of fluid	m
e	thickness	m
f	frequency	s^{-1}
H	$= h_p \sigma_s$ volumetric heat transfer coefficient	$W \cdot m^{-3} \cdot K^{-1}$
$\dot{H}$	enthalpy flow rate	W
h	heat transfer coefficient	$W \cdot m^{-2} \cdot K^{-1}$
Inef	inefficiency of regenerator	
j	first root of $j^2 = -1$	
K_n	$= \frac{L_p}{L_c}$ Knudsen number	
k	thermal conductivity	$W \cdot m^{-1} \cdot K^{-1}$
L, l	length	m
$\overline{M}$	molecular mass	$kg \cdot mole^{-1}$
$\dot{m}$	mass flow rate	$kg \cdot s^{-1}$
N	number of fins	
N_u	Nusselt number	
p	Laplace parameter	s^{-1}
p, q	constants Eq. (23)	
P	pressure	Pa
P_r	$= \frac{c\mu}{k}$ Prandtl number	
q	power density	$W \cdot m^{-3}$
$\dot{Q}$	heat flow	W
r	half diameter	m
r	$= \overline{R}/\overline{M}$	$J \cdot kg^{-1} \cdot K^{-1}$
r_1, r_2, r_3	roots of Eq. (A.15)	
$\overline{R}$	thermodynamic constant	$J \cdot mole^{-1} \cdot K^{-1}$
R_c	characteristic time (A.2)	
Re	$= \Delta P/\dot{m}$ hydraulic resistance	$m^{-1} \cdot s^{-1}$
Re_h	$= \frac{\dot{m} D_h}{\mu S_{\text{pass}}}$ Reynolds number	
S	area	m^2
T	temperature	K
t	time	s
u	gas velocity	$m \cdot s^{-1}$
U	amplitude velocity	$m \cdot s^{-1}$
V	volume	m^3
w	width	m
x	longitudinal coordinate	m

Greek symbols

δ	thickness	m
Δ	difference	
ε	void fraction	
γ	isentropic coefficient	
η_s	fin weighted factor	
η_a	slab efficiency	
λ	gap between fins	m
μ	dynamical viscosity	$kg \cdot m^{-1} \cdot s^{-1}$
Φ	thermal flux density	$W \cdot m^{-2}$
ρ	density	$kg \cdot m^{-3}$
θ	phase lag	rad
θ	non-dimensional temperature	
σ	specific area	m^{-1}
τ	period, or non-dimensional time	
ω	pulsation	$rad \cdot s^{-1}$
χ	non-dimensional longitudinal variable	

Subscripts and superscripts

1	first order periodic perturbation
1, 2	indices for notation Eq. (22)
a	ambient
c	characteristic, cold zone
ext	exterior
f	fin
g	gas
gl	glass
h	hydraulic, hot zone
imp	impulse response
inlet	inlet of the gas
int	interior
k	thermal
loss	conductive thermal losses
lre	regenerator outlet
max	maximal without losses
net	tacking losses into account
p	particle or at constant pressure
pass	passage
re	regenerator
s	solid
shut	with shuttle effect
Si	silicon
t, tub	tube
tot	total
v	viscous
w	wall
$\bar{x}$	spatial average value of x
$\hat{x}$	Laplace transform of x
$\langle x \rangle$	time average value of x
$\tilde{x}$	time fluctuating amplitude of x

to those of an electronic component. Nevertheless, these devices also require a compressor or a rotating valve to generate a pressure fluctuation that may introduce some trouble in the electronic component functioning; but, fortunately, the pressure generator of such systems can be easily split. Pulse Tube Refrigerators (PTR) have been strongly studied for about ten years and they already proved their interest in various domains such spatial applications, infrared or ul-

traviolet sensors cooling, or SQUID or CDMOS cooling [3–8]. Among the different PTR types, the geometry introduced by Mikulin [9] in 1985 with an orifice and a reservoir (OPTR) appears to be particularly efficient at low temperature. Indeed, a temperature level near 20 K was reached with a single stage and 4 K with a second one. Other adaptations of PTR with several fluid inlets (DIOPTR) have been studied by Zhou [10] since 1990. Many current researches propose to use gasses mixtures or concern the introduction of different original geometries (e.g., *U* shape or coaxial configurations) [11–13]. Others put forward the use of electric gates for controlling the fluid flow through the different parts of the cooler [14]. In this paper, the authors suggest to use the techniques of electronic industry to design and realize a micro-cooler only made of glass and of silicon. The design of the micro-device is presented as an extension of results obtained in previous researches [15] concerning a small OPTR realized with classical techniques of manufacturing (classical scale). Nevertheless, the design of heat exchangers is more difficult at micro-scale. It is achieved by considering the transient thermal response of these small elements of complex geometry. A detailed presentation of the theoretical procedure is proposed. Lastly a complete micro-cooler has been built and the first experimental results are presented.

2. Principle of the double inlet orifice pulse tube refrigeration

Among various types of PTR, the simple Orifice Pulse Tube Refrigerator (OPTR) and the Double Inlet Orifice Pulse Tube Refrigerator (DIOPTR) allow to reach good performances. This kind of devices are generally filled with helium under pressure and (case of this paper) are constituted of the following basic parts (see Fig. 1):

- a compressor without valve for generating sinusoidal pressure variations,
- a first heat exchanger to evacuate the heat generated during the compression,
- a thermal regenerator (similar to that of Stirling machines),
- a second exchanger in the cold zone,
- the tube itself,
- and a last heat exchanger for extracting heat from the hot zone.

The system is linked up to a gas reservoir by means of a capillary tube. The reservoir is big enough to keep an almost constant pressure. The capillary tube is essential to ensure the refrigerator in good working order: this element allows to adjust the phase lag that occurs between the pressure fluctuation and the gas velocity; this influences the cooling production in a very sensible way. Another optional capillary tube may be used to directly link the regenerator inlet to the pulse tube outlet in order to achieve better efficiency of the regenerator. The use of a by-pass for the DIOPTR does not modify the global principle of the OPTR but allows to increase the cooling production. This part will be discussed later in this paper. In fact, three physical phenomena predominate in the functioning of a pulse tube like an OPTR or DIOPTR:

- The phase lag between the evolutions of the pressure and of the mass flow rate (velocity): because the cooling production depends directly of the product of the gas velocity by its pressure. Indeed, in the case of periodic harmonic variations Eq. (1), the expression Eq. (2) of the temporal average of the mechanical work received

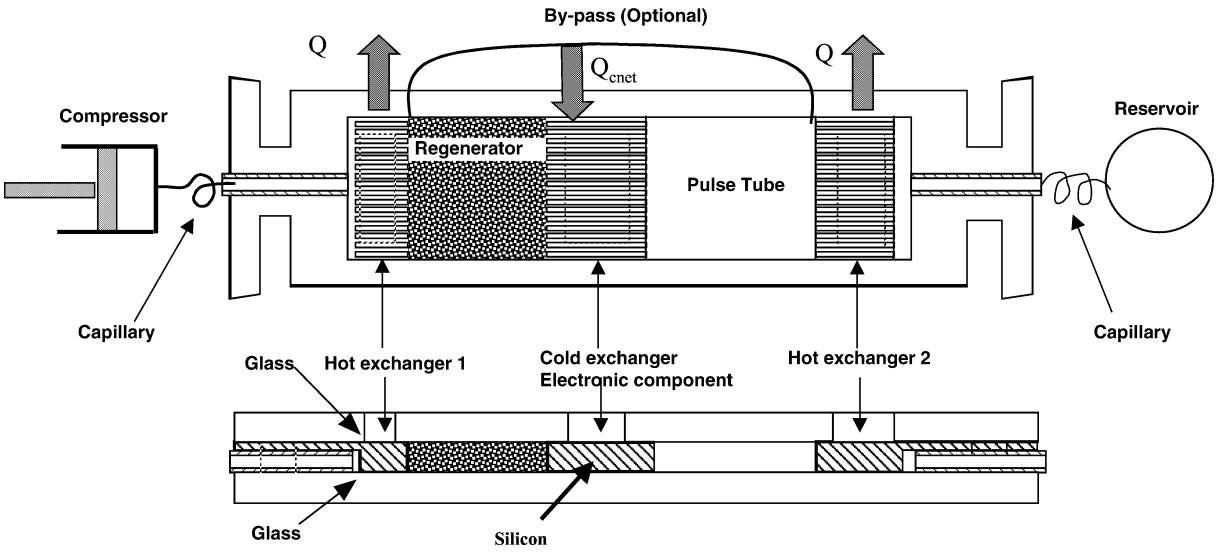

Fig. 1. Schematic representation of the double inlet orifice pulse tube refrigerator.

by the gas during a pressure variation cycle clearly indicates the essential influence of this phase lag.

$$\dot{m} = m_1 \cos \omega t \qquad P = \overline{P} + P_1 \cos(\omega t - \theta) \tag{1}$$

$$\langle \dot{W} \rangle = \frac{1}{\tau} \int_0^{\tau} P \frac{\mathrm{d}V}{\mathrm{d}t} \,\mathrm{d}t = \frac{1}{2} \frac{r\overline{T}}{\overline{P}} m_1 P_1 \cos\theta \tag{2}$$

In Eq. (1), one supposes that a periodic pressure perturbation of amplitude P_1 is imposed by the pressure generator, the inflating pressure being $\overline{P}$ and the phase lag with respect to the mass flow rate $\dot{m}$ is θ. In a free thermodynamic system, the energy transported by the gas is either kinetic energy or potential energy (pressure). This leads to a natural phase lag $\theta = \pi/2$ between velocity and pressure, hence the mean thermodynamic effect along a period equals zero. The use of a capillary tube permits to modify this phase lag in order to generate a thermal effect actually.

– The Surface Heat Pumping effect between the oscillating gas flow and the pulse tube wall that consists globally in an energy transfer between the cold zone to the hot zone [16]. During the compression phase, the gas temperature increases while moving in the tube towards the hot zone. Therefore, the thermal exchanges are favored from the gas to the external walls. Similarly, during the expansion, the gas temperature decreases while moving towards the cold zone so that the final temperature is lower than the initial temperature. Globally, this phenomenon generates a temperature gradient along the pulse tube (in the gas and also in the tube wall). As a result, step by step, the gas loads thermal heat near the cold zone and transports it to the hot exchanger: the global axial enthalpy flux through a section S appearing along the tube, is defined by Eq. (3).

$$\langle \dot{H} \rangle = \int_S c_{pg} \langle \rho_g u T \rangle \,\mathrm{d}S \tag{3}$$

where helium is considered as a perfect gas so that the enthalpy depends only on the temperature [17].

– The presence of a thermodynamic discontinuity: in the case of an ideal regenerator (infinite thermal capacity and perfect thermal exchanges between the gas and the solid matrix), the gas temperature is constant so no enthalpy flux can be observed. On the contrary an enthalpy flux occurs through the tube actually, so a thermodynamic discontinuity takes place at the outlet of the regenerator due to the sudden change of medium. This phenomenon induces a local temperature decrease and explains the cold zone location at this place.

By considering these effects, the maximal cooling production (that could be available for cooling an electronic component if no thermal loss occurred) [15,18], can be estimated with Eq. (4) deduced from the temporal average of the gas enthalpy variation during a whole cycle at the cold exchanger inlet:

$$\langle \dot{Q}_{c\max} \rangle = \frac{\omega c_{pg}}{2\pi} \int_{t_0}^{t_0+\pi/\omega} \dot{m}(t) \big(T_c - T_{\mathrm{lre}}(t)\big) \,\mathrm{d}t \tag{4}$$

where t_0 corresponds to the instant when the mass flow rate in the cold exchanger becomes null so that the fluid begins entering from the tube to the cold exchanger. $t_0 + \pi/\omega$ is the instant when the mass flow rate is null again. The cooling effect takes place between these two characteristic instants.

Of course the cooling production given by Eq. (4) does not correspond to reality. On the one hand, the regenerator is not ideal and its temperature is not uniform actually. The existing temperature gradient generates longitudinal thermal losses (heat conduction) which implies a decrease of the cooling production. Besides the regenerator efficiency is not 1 (non-perfect heat transfer, irreversibility and non-infinite thermal inertia) and the regenerator is not adiabatic, thus additional transversal losses are to be considered. On the other hand, the thermal gradient between the hot zone (hot exchanger) and the cold zone is important especially in micro-devices (typically a few 1000 $\mathrm{K{\cdot}m^{-1}}$). All these phenomena introduce losses that are to be taken into account for estimating the effective cooling production, particularly at micro-scale. Moreover, if the gas displacement is greater than the tube length, it may bring a heat quantity directly from the hot exchanger to the cold zone (shuttle effect). Other losses with the surroundings may be important especially when low temperatures are reached and when radiation effects become preponderant. Fig. 2 gives a representation of the global thermal balance of the cold zone. Finally, the net cooling power can be summarized with Eq. (5):

$$\langle \dot{Q}_{c\,\mathrm{net}} \rangle = \langle \dot{Q}_{c\max} \rangle - \langle \dot{H}_{\mathrm{re}} \rangle - \langle \dot{Q}_{\mathrm{loss}} \rangle - \langle \dot{Q}_{\mathrm{shut}} \rangle \tag{5}$$

$\langle \dot{H}_{\mathrm{re}} \rangle$: designates the enthalpy flux through the regenerator (null if the gas flowing through the regenerator remains isothermal perfectly).

$\langle \dot{Q}_{\mathrm{loss}} \rangle$: is the heat quantity due to thermal conduction in solid part.

$\langle \dot{Q}_{\mathrm{shut}} \rangle$: corresponds to the heat quantity directly brought by the gas when alternatively displacing between the cold and the warm zones.

The work presented in this paper focuses neither on the calculus of these terms nor on the optimization of the net cooling power; other papers concerning these parts have been published [15] and some are about to be published.

In a first step, for designing the cooler, all exchangers are supposed to be perfect. This simplification allows to evaluate the main functioning conditions, meaning pressures, mass flow rates and other governing parameters. Then, in a second step, the final design is based on the results obtained previously and on different considerations about the actual behavior of heat exchangers.

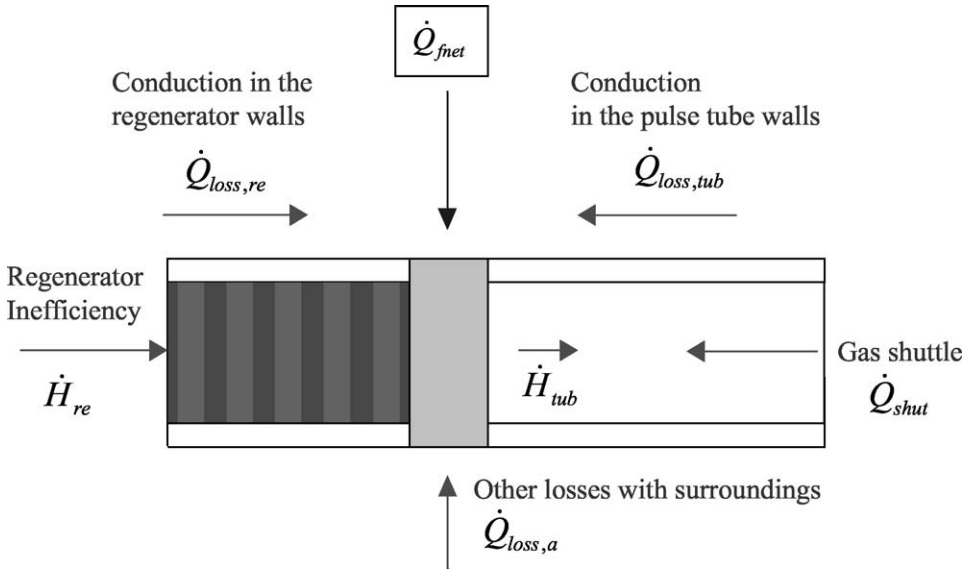

Fig. 2. Thermal balance of the cold zone.

3. Miniaturization of the refrigerator: from classical technology to "silicon" technology

By considering the previous remarks on the Pulse Tube principle, miniaturization appears to be a tricky challenge. At small scale, if the temperature levels remain similar to those observed at classical scale, the distance between the different parts (hot and cold) decreases so the temperature gradient (hence $\langle \dot{Q}_{\text{loss}} \rangle$) strongly increases. This basic observation indicates that whatever the geometry used, the thermal losses will be important. Therefore, the authors have first adjusted and completed the theoretical and numerical models [15,18] they had previously established for usual scale. In addition, experimental investigations were achieved on a commercial miniaturized pulse tube (provided by Thales Cryogénie France). Fig. 3 shows an image of this device obtained by using classical technologies of fabrication and machining: like devices described in [1–6], it is relatively small; however it does not still correspond to the scale of an electronic component. Nevertheless, it can be used as an intermediate device between usual cooler and the ideal miniaturized machine. An example of typical results obtained with this cooler during an experiment in transient regime is reported on Fig. 4. The maximal cooling power is about 4 W at 273 K and the lowest temperature reached by this system is 110 K (with a moderate inflating pressure of helium about 1.2 MPa and an operating frequency of 50 Hz). The performances also depend of the swept volume of the compressor (not represented in the photograph of Fig. 3) which is linked to the passive module at the extremity thanks to a capillary. This compressor is a high technology product of confidential geometry developed by Thales Cryogénie France.

In fact, to reduce the pulse tube dimensions for adapting it to an electronic component, prior to discuss the theoretical analysis or the modeling procedure, it is capital to consider

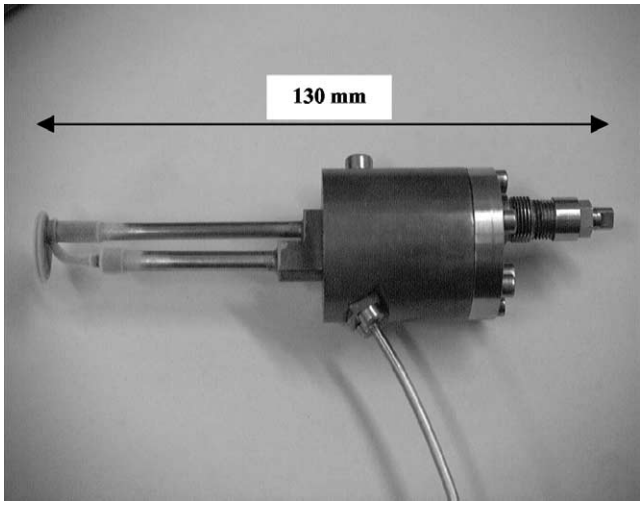

Fig. 3. Miniaturized pulse tube of classical technologies Thalès Cryogénie France.

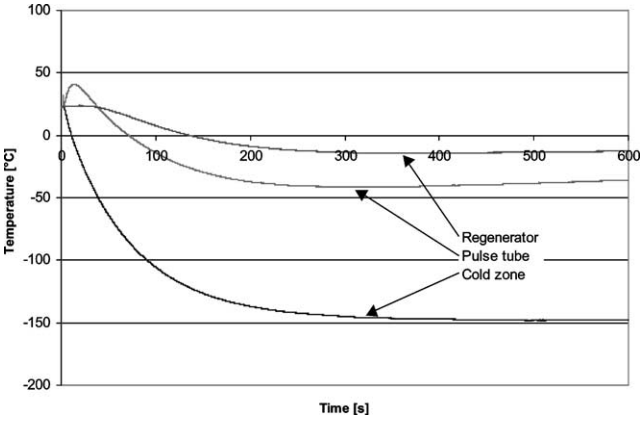

Fig. 4. Temperature histories in the miniaturized pulse tube of classical technologies (inflating pressure: 1.2 MPa, pulsating frequency: 50 Hz).

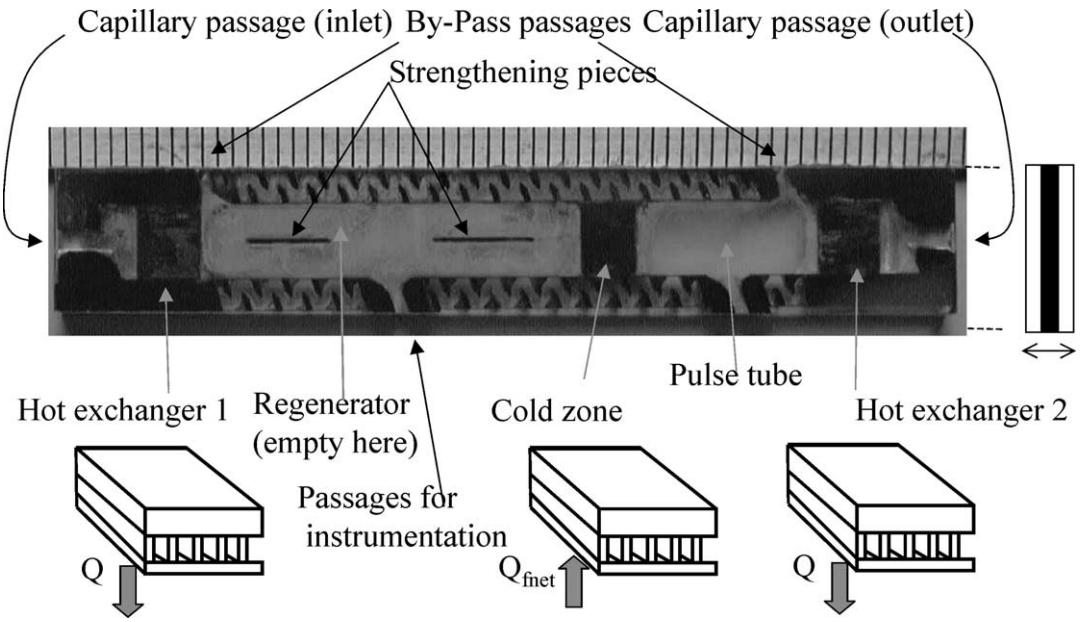

Fig. 5. Global view of the micro DIOPTR refrigerator passive module.

the question of the micro-cooler fabrication. Indeed, because many problems appear at small scale (including helium leakage, friction, micro machining, etc.) classical mechanical technologies do not operate any more. When reducing the cooler dimensions, the tube diminishes but the heat exchangers and the regenerator have also to diminish. Thus, the challenge is to find or develop a relevant process for fabricating such micro-elements. In this paper, the authors propose to test the technology usually used in electronic industry. The silicon is a well-known material and different techniques can be used to machine it (e.g., etching). Moreover, the silicon of orientation 110° can be gathered with a specific glass by using an electric field. So, the association of these two basic elements, silicon and glass, allows to built very small three-dimensional structures similar to that of a pulse tube. In this paper, only the miniaturization of the passive part of the pulse tube (passive module) is presented, the miniaturization of the compressor seems also possible but it has not been considered yet; a set of classical commercial compressors, initially built for mini Stirling cooler can be used: different swept volumes of a few cm^3 are available.

Fig. 5 presents the architecture of the micro-miniature passive module. It was designed from the results obtained with the previous miniature pulse tube based on classical mechanical technologies. This new micro-module is made of silicon and glass. It is constituted of a silicon slab (spacing slab, see Fig. 1) encapsulated between two glass slabs. The silicon is etched by means of chemical techniques in order to create the different parts of the pulse tube (Figs. 1 and 2): three heat exchangers, the inlet and the outlet of the module, two volumes for the regenerator and the pulse tube itself. Additional structures, canals and orifices, are performed in order to introduce temperature sensors or to fill the regenerator with a porous medium (stack of glass

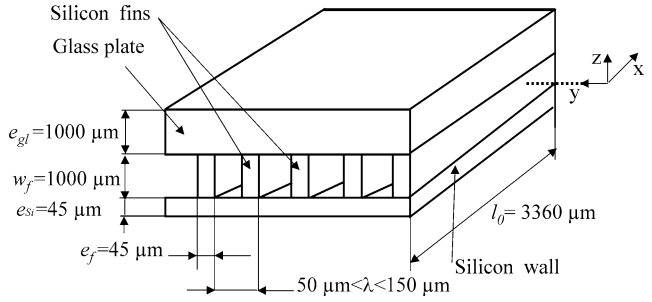

Fig. 6. Schematic geometry of micro heat exchangers.

beads).The micro-fabrication techniques allow to built very compact heat exchangers based on a great number of fins (a few dozen) to ensure a great internal exchange surface. Fig. 6 gives the mains geometrical characteristics of these devices. To permit heat transfers with the ambient air or with an electronic component, one of the faces (made of glass) of each exchanger is carved by ultrasonic machining so that only a thin silicon layer is conserved (45 µm). When the refrigerator device is operating, two radiators are adapted on the hot exchangers 1 and 2 in order to maintain their temperature very close to that of the surroundings. The electronic component to be cooled is directly located on the silicon matrix of the cold exchanger (carved side). In order to conserve a good control on the internal geometry of the heat exchangers, the minimal fin thickness is fixed to 45 µm and the gap between fins is adjustable in a range from 50 to 150 µm. In fact, these dimensions do not correspond to the limits of the silicon carving process but because silicon is not isotropic, the chemical etching efficiency is not the same in all directions. A typical example of realization is shown on Fig. 7.

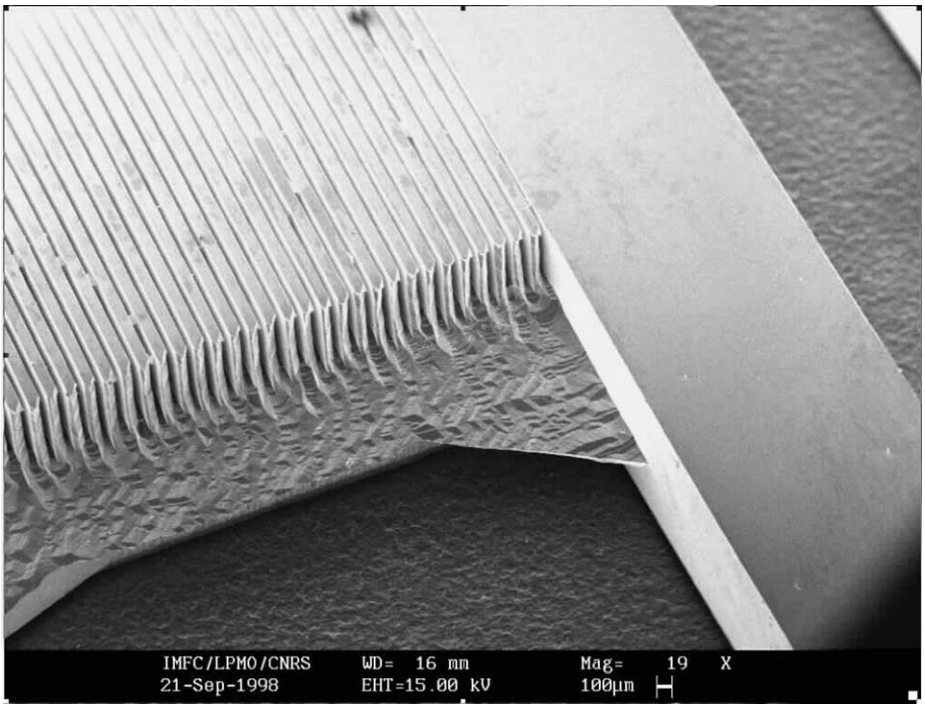

Fig. 7. Details of the walls and the structure of heat exchangers.

Table 1
Thermophysical properties of the DIOPTR materials

	Silicon	Glass
Thermal conductivity K ($W{\cdot}m^{-1}{\cdot}K^{-1}$)	270 at 200 K 150 at 300 K	1.13 at 273 K
Thermal capacity C ($J{\cdot}cm^{-3}{\cdot}K^{-1}$)	1.66 at 300 K	1.68 at 300 K

Table 1 summarizes the thermo-physical properties of the materials [19] used in this passive micro-module. One can observe the great values of the thermal conductivity especially for the silicon: this is a good point for improving thermal exchanges in heat exchangers however it becomes a handicap for the structure of the refrigerator because the thermal losses are favored. To limit the influence of this major problem, the lateral walls made of silicon are designed as thick as possible: in fact, they are constituted of two partitions of 40 µm thick separated by an air layer of 2000 µm (lateral structure on Fig. 5). To ensure the global mechanical resistance of the module, straightening pieces of 450 µm thick are added into the regenerator and the gas tube. The glass slabs thickness is restricted to 1 mm, this value being sufficient to support an inflating pressure about 1.2 MPa.

The transversal geometrical characteristics indicated previously have been chosen from considerations on the available thickness of the silicon slab and on the mechanical resistance of the glass. Indeed, for this study, it is not possible to create new specific elements of specific dimensions (e.g., specific thickness): all the fabricating process has to be based on elements commonly used in the microelectronic industry. Therefore, another consideration that may limit the miniaturization of the system is the thickness of the thermal and dynamic boundary layers given by Eq. (6). With helium and considering the following operating conditions, frequency: 50 Hz, inflating pressure: 1.2 MPa, temperature: 300 K, these viscous and thermal boundary layers can be estimated by [20]:

$$\delta_v = \sqrt{\frac{2\mu_g}{\rho_g \omega}} = 0.268\ \text{mm} \quad \text{and}$$
$$\delta_k = \sqrt{\frac{2k_g}{\rho_g c_{pg} \omega}} = 0.327\ \text{mm} \tag{6}$$

This evaluation is most important for estimating the minimum transversal dimension of the pulse tube zone (see Fig. 1): indeed, in this part of the cooler, a maximal temperature fluctuation is necessary for obtaining a cooling effect, so all geometrical dimensions have to be larger than the double of the thermal boundary layer thickness. Similarly in order to limit pressure losses, all dimensions have to be greater than the dynamic boundary layer thickness too. Besides, the length of the pulse tube has to be sufficient for avoiding "shuttle effects": in fact, if the pulse tube is not long enough, the periodic displacement of the gas may be longer than the pulse tube; then, the warm zone and the cold zone may be directly linked and the cooling production vanishes. In that case, shuttle effects occur and increase the thermal losses $\langle \dot{Q}_{\text{shut}} \rangle$ of the system. To limit this problem, the length of the gas tube must be greater than the total gas displacement

occurring during a period. Thereby Eq. (7) should be verified.

$$l_t \gg displ \approx \frac{2}{\omega}U = \frac{8m_1}{\pi\rho_g\omega d_t^2} \tag{7}$$

Finally, in the pulse tube, the thermal effects and the aerodynamic effects are simultaneously improved when the geometrical dimensions are increased. However, for the global refrigerator device, the pulse tube appears as a dead volume so, it has not to be too much important otherwise the pressure amplitude may vanish. As a result, a compromise between the thermal effects and the pressure amplitude has to be found.

In the heat exchangers and especially in the regenerator ($\langle \dot{H}_{\mathrm{re}} \rangle$ minimal), the transversal dimensions have to be similar or smaller than the thermal boundary layer thickness. Indeed, in an ideal regenerator, the longitudinal thermal gradient is null, so the gas temperature is very close to that of the solid matrix. This can be achieved only if the characteristic dimension is smaller than the thermal boundary layer thickness. Unfortunately, when diminishing this parameter, the pressure losses increase dramatically: again a compromise has to be obtained between the thermal effect and the pressure amplitude.

The pneumatic links between the passive module and the compressor or the reservoir are assumed by capillaries made of stainless steel which internal diameters are 0.3 and 0.7 mm, respectively.

4. Micro heat exchangers design

As explained before, the etching techniques used with silicon allow to create very thin three-dimensional structures. This advantage is very interesting to make and integrate the small heat exchangers to the passive module. By the way, the spacing slab is used to realize three sets of parallel blades in the silicon, creating the three heat exchangers. However, two aspects must be carefully observed: the creation of a sufficient heat transfer surface and the minimization of energy losses due to friction. In fact , the design of the micro heat exchangers is quite difficult because they operate in periodic regime and also because of the lack of knowledge concerning thermal and aerodynamic effects at small scale. Moreover, the use of a proportional relation based on the classical DIOPTR dimensions (first step of miniaturization tested previously) is not efficient any more: both the heat transfer and the flow resistance have to be considered carefully. But, no available research has been done in the field of micro heat exchangers design in the case of periodic compressible flow. Therefore, prior to propose a theoretical formulation, it is important to evaluate the relevancy limits of the classical formulations when applying them at a small scale problem.

For fluid flows through conduits, one usually admits that there is a transition from the Poiseuille continuous regime to the Knudsen molecular regime as soon as the free average course L_p of the gas molecules becomes important in front of the characteristic dimension L_c of the system (diameter for a tube). The criterion is the non-dimensional Knudsen number compared to unity [21]:

$$K_n = \frac{L_p}{L_c} \ll 1 \tag{8}$$

The kinetic theory of gases allows to calculate it by using the following expression [21]:

$$L_p = \frac{T}{P}3k_g(\gamma - 1)\sqrt{\frac{\pi\overline{M}}{8T\overline{R}}} \tag{9}$$

In the considered situation, the free average course is about 66 nm while the minimal machined dimension of passages for the fluid is about 50 μm. The conclusion of this basic approach is the usual models still remain valid because $K_n \approx 10^{-4}$.

According to [22], the efficiency of heat exchangers is related to the ratio of the thermal diffusivity of the material that the exchanger walls are made of to that of the fluid; as this ratio gets smaller, the axial conductive losses $\langle \dot{Q}_{\mathrm{loss}} \rangle$ decrease. Then, in the case of an inflating pressure of 1.2 MPa, the authors propose to apply a ratio of the length to the hydraulic diameter following Eq. (10):

$$\frac{l_t}{D_h} \gg \frac{a_w}{a_g} = 0.05 \quad \text{for the glass, and 0.86 for the silicon} \tag{10}$$

The problem is not very accurate in the case of the cold and hot exchangers, their dimensions being similar to that of the pulse tube (1×4.5 mm). On the contrary, in the regenerator, the porous matrix is constituted of a stack of glass beads and the envelop is made of Pyrex. In fact, in the regenerator, the fluid flows through very small passages hence inducing subsequent pressure losses. Again, the problem is to reach optimal thermal effects while inducing minimal pressure losses.

4.1. Global model of pressure losses for static and dynamic regimes

It is easy to understand that pressure losses in exchangers decrease the pressure amplitude in the pulse tube and cause the net output power $\langle \dot{Q}_{c\,\mathrm{net}} \rangle$ of the refrigerator to fall down. But it appears that estimating the pressure losses is a very hard task in oscillating systems and especially in the case of compressible gases. According to scientific literature, no specific research related to this problem has been ever achieved completely; nevertheless, the calculation remains possible in the case of non-oscillating flows, even at small scale. Therefore the authors evaluate the pressure drop by considering either the mean velocity or the maximal velocity of the oscillating flow to achieve their calculations.

Table 2
Values of coefficients a, b and c in Eq. (12)

Model	a	b	c
Hagen–Poiseuille steady circular tube	64	0	1
Hagen–Poiseuille steady rectangular tube	68.5	0	1
Blasius steady circular tube	0.313	0	0.25
Prandtl–Karman steady circular tube	0	Depend of roughness	0
Turbulent steady rectangular tube	0.31	0	0.25
Kozeny steady porous	$a = 72\kappa_0 \frac{(1-\varepsilon)^2}{\varepsilon^2} \frac{D_h^2}{d_p^2} = 32\kappa_0$	0	1
Ergun steady porous	$a = 72\kappa_1 \frac{(1-\varepsilon)^2}{\varepsilon^2} \frac{D_h^2}{d_p^2} = 133$	$b = 12\kappa_2 \frac{(1-\varepsilon)}{\varepsilon} \frac{D_h}{d_p} = 2.33$	1
Tanaka periodic	175	1.6	0

Case $\varepsilon \frac{d_p}{D_h} Re_h < 10$: κ_0 is a shape factor ($3.6 < \kappa_0 < 5$). It is 4.8 for spheres (Kozeny).

Case $\varepsilon \frac{d_p}{D_h} Re_h > 10$: $\kappa_1 = 4.16$, $\kappa_2 = 0.29$ (Ergun).

In static regime, the pressure losses in a conduit are usually estimated by using the pressure drop factor given by Eq. (11) [23,24].

$$C'_f = \frac{2\Delta P D_h}{\rho_g U^2 L} \tag{11}$$

In any case, C'_f is generally estimated as a function of the Reynolds number based on the hydraulic diameter D_h . The Hagen–Poiseuille model is used for the laminar regime and the Blasius and Prandtl–Karman models are applied to the smooth and rough turbulent regimes respectively. Usually, the mathematical form of Eq. (12) is used. The parameters a, b and c are variable coefficients to be determined.

$$C'_f = \frac{a}{Re_h^c} + b \tag{12}$$

The Reynolds number definition is given by [23,24]:

$$Re_h = \frac{\rho_g u D_h}{\mu_g} = \frac{\dot{m} D_h}{\mu_g S_{\text{pass}}} \tag{13}$$

For a porous medium made of a stack of beads, a similar formulation can be used, however the hydraulic diameter is evaluated by [23,24]:

$$D_h = \frac{2}{3} \frac{\varepsilon d_p}{(1-\varepsilon)} \tag{14}$$

where ε is the void fraction of the porous phase and d_p the beads diameter.

Table 2 summarizes the values of the coefficients $\{a, b, c\}$ of Eq. (12) for different situations [25]. In order to evaluate the relevance of these correlation, different experiments in static regime have been performed on the micro-module. The procedure and the materials will be briefly described in Section 5. Two cases have been considered: on the one hand, the pressure drops introduced by the whole passive module ΔP_{tot} (exchangers + regenerator without glass beads + capillaries), on the other hand the pressure drop induced by the only regenerator, with or without the beads, ΔP_{re}. The results reported on Fig. 8 indicate the pressure drops increase proportionally with the mass flow rate, except for weak values where unidentified phenomena occurs. The regenerator is responsible of a third of the total losses and when it is filled with glass beads, the pressure drop increases in a range of 15 to 20%. These data show that the classical Ergun porous steady model remains valid at this small scale and at sufficient porous Reynolds number, but the void fraction appears to have a dramatically strong influence. Because of the random arrangement of beads, it is also quite difficult to obtain an accurate value of ε (from 0.33 to 0.45). Fig. 9 represents the evolution of the hydraulic resistance $(\Delta P_{\text{re}}(\text{withbeads}) - \Delta P_{\text{re}}(\text{withoutbeads}))/\dot{m}$ of the glass beads calculated for experimental and calculated results using the Ergun model and Table 2 for three values of the void fraction ε.

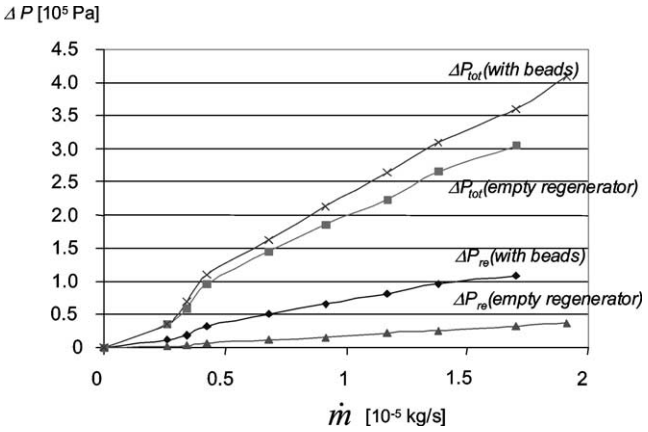

Fig. 8. Influence of the stack of beads. Global pressure drop measurements in the passive module with mass flow rate into the regenerator (static flow).

Therefore a new specific experiment is required for evaluating the void fraction of the regenerator for each new module. Besides, another study has been dedicated to the junctions capillaries effects. Fig. 10 compares the experimental results for a permanent gas flow with the results of the various classic models of Table 2: a good accordance is obtained for various capillaries (0.3 to 1 mm diameter), especially for a Reynolds number either minor than 1000 (laminar-Poiseuille correlation), or greater than 4500

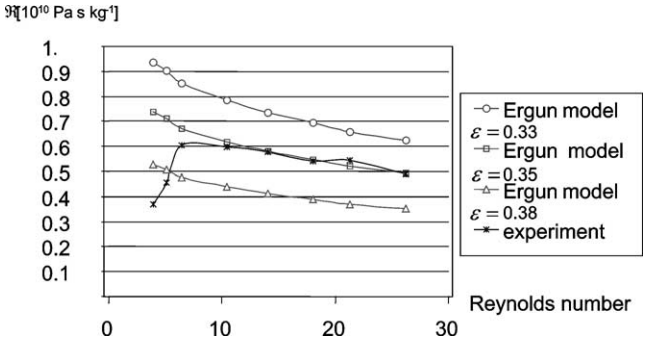

Fig. 9. Comparison between models and experiments of the hydraulic resistance $\Re = \frac{\Delta P}{\dot{m}}$ of the stack of beads in the regenerator with Reynolds number ($\varepsilon = 0.33$, 0.35, 0.38, static regime).

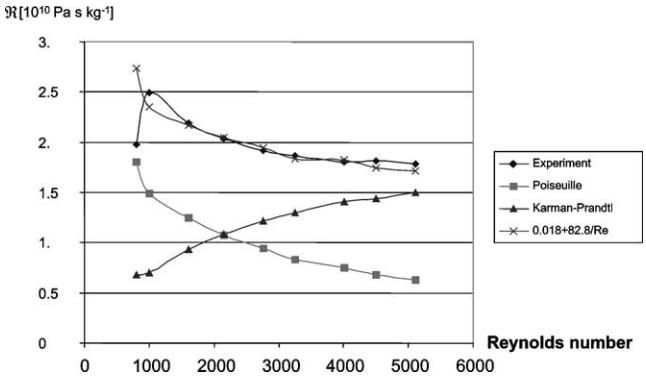

Fig. 10. Comparison between models and experiments of the hydraulic resistance $\Re = \frac{\Delta P}{\dot{m}}$ of a capillary of 0.3 mm diameter with Reynolds number (static regime).

(turbulent-Karman–Prandtl correlation with $C'_f = 0.0375$). The authors have obtained an experimental correlation corresponding to Eq. (12) where $a = 82.8$, $b = 0.018$ and $c = 1$. It is particularly relevant for the intermediate values of the Reynolds numbers in a range from 1000 to 5000.

In dynamic regime, very few studies for modeling the pressure amplitude variations exist [23,24]. Again the experimental way appears to be the best solution for obtaining some indications, especially at small scale. The pressure measurements at the inlet and the outlet of the passive module are reported on Fig. 11. For all the operating frequencies used during the tests, the pressure amplitudes are not in good accordance with the prediction of the authors models [15,18] using Tanaka values listed in Table 2 (Fig. 12). Indeed, the pressure drop between the regenerator extremities are greater than the calculated values actually. In fact, the pressure amplitude at the outlet is a linear function of the inflating pressure in estimations; but the measured pressure amplitude is 50% lower than the calculated value approximately. Concerning the pressure amplitude at the module inlet, experimental and calculated estimations are in good accordance but an important unexplained collapse of the pressure amplitude is observed for an inflating pressure about 1 MPa.

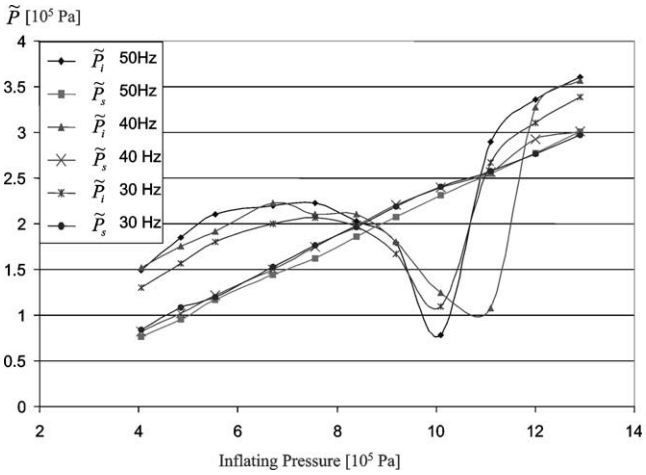

Fig. 11. Inlet and outlet pressure amplitude experimental estimation in the passive module measurement (dynamic regime).

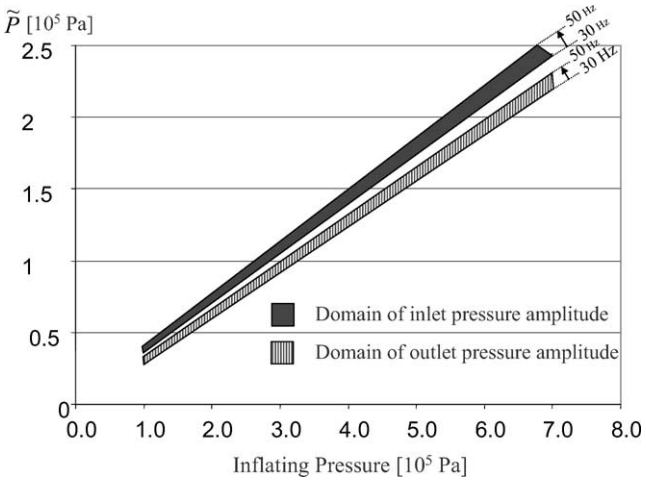

Fig. 12. Inlet and outlet pressure amplitude theoretical estimation in the passive module (dynamic regime).

4.2. Transitory thermal response of the regenerator and the heat exchangers

4.2.1. Thermal modeling of the regenerator

When operating, the temperature, pressure and mass flow rate are not constant values at the regenerator extremities and to date, the modeling of its transitory thermal behavior is an unexplored problem at small scale. Moreover, it is necessary to take into account the thermal influence of the regenerator envelope, involving considerations on thermal exchange with the surroundings and thermal conduction through the walls. The authors have already solved the problem of the transitory response to a step excitation in the case of mini regenerator of cylindrical geometry [26]. In this model, the mass flow rate, the density and the pressure are supposed to be constant values; thus, by using classical basic equations of fluid mechanics and heat transfer, a system of three equations, Eq. (15), for the gas, the porous matrix and the envelope can be obtained.

$$\rho_x c_x\left(\frac{\partial T_x}{\partial t}+\frac{U_x}{\varepsilon}\frac{\partial T_x}{\partial x}\right)=q_x+k_x\left(\frac{\partial^2 T_x}{\partial r^2}+\frac{1}{r}\frac{\partial T_x}{\partial r}\right)\quad(x=g,s,w)\tag{15}$$

where $U_s=U_w=0$.

The boundary conditions are:

– for $r=0$; the gas and the matrix temperature repartitions are of axial symmetry:

$$\left.\frac{\partial T_g}{\partial r}\right|_{r=0}=0\quad\text{and}\quad\left.\frac{\partial T_s}{\partial r}\right|_{r=0}=0\tag{16}$$

– for $r=r_{\text{int}}$; at the wall, the thermal flux through the gas equals the one in the wall. Besides the thermal flux between beads and the wall is null because of their small contacting surface:

$$k_g\left.\frac{\partial T_g}{\partial r}\right|_{r=r_{\text{int}}}=k_w\left.\frac{\partial T_w}{\partial r}\right|_{r=r_{\text{int}}}\quad\text{and}\quad k_s\left.\frac{\partial T_s}{\partial r}\right|_{r=r_{\text{int}}}=0\tag{17}$$

– for $r=r_{\text{ext}}$; the thermal losses with the surrounding are expressed as following:

$$k_w\left.\frac{\partial T_w}{\partial r}\right|_{r=r_{\text{ext}}}=h_{\text{ext}}(T_a-T_w|_{r=r_{\text{ext}}})\tag{18}$$

The initial condition for the gas and the solid is supposed uniform and equal to surrounding temperature when the step response is studied.

In this model, the authors make the assumption that the longitudinal thermal conduction through the gas and the matrix is negligible. Then, the three previous equations are averaged along the radial direction in order to provide a one-dimensional formulation of the problem only depending on the axial coordinate x.

$$\left(\varepsilon\frac{\partial\overline{T}_{g,\text{re}}}{\partial t}+\overline{U}\frac{\partial\overline{T}_{g,\text{re}}}{\partial x}\right)=\frac{\sigma_s h_p}{\rho_g c_g}\left(\overline{T}_{s,\text{re}}-\overline{T}_{g,\text{re}}\right)+\frac{\varepsilon\sigma_1 h_{\text{int}}}{\rho_g c_g}\left(\overline{T}_{w,\text{re}}-\overline{T}_{g,\text{re}}\right)\tag{19}$$

$$(1-\varepsilon)\frac{\partial\overline{T}_{s,\text{re}}}{\partial t}=\frac{\sigma_s h_p}{\rho_s c_s}\left(\overline{T}_{g,\text{re}}-\overline{T}_{s,\text{re}}\right)\tag{20}$$

$$\frac{\partial\overline{T}_{w,\text{re}}}{\partial t}=\frac{\sigma_{\text{ext}}h_{\text{ext}}}{\rho_{w,\text{re}}c_{w,\text{re}}}\left(T_a-\overline{T}_{w,\text{re}}\right)+\frac{\sigma_2 h_{\text{int}}}{\rho_{w,\text{re}}c_{w,\text{re}}}\left(\overline{T}_{g,\text{re}}-\overline{T}_{w,\text{re}}\right)+\frac{k_{w,\text{re}}}{\rho_{w,\text{re}}c_{w,\text{re}}}\frac{\partial^2\overline{T}_{w,\text{re}}}{\partial x^2}\tag{21}$$

where specific areas are defined by:

$$\sigma_s=(1-\varepsilon)\sigma_p=(1-\varepsilon)\frac{6}{d_p},\qquad\sigma_1=\frac{S_{\text{int}}}{V_{\text{int}}}\qquad\sigma_{\text{ext}}=\frac{S_{\text{ext}}}{V_w},\qquad\sigma_2=\frac{S_{\text{int}}}{V_w}\tag{22}$$

S_{int}, S_{ext}, V_{int}, V_w, designate the internal and the external thermal exchange area, the gas volume and the volume of the envelope, respectively.

Three global thermal coefficients have been introduced: the first one h_{ext} characterizes the external losses between the envelope and the surroundings, the second one h_{int} is related to the exchanges between the gas and the internal surface of the envelope, and the last one h_p is dedicated to the thermal exchanges between the gas and the matrix. In the case of a stack of beads, no classic correlation is available for estimating h_{int} and h_p. However, Refs. [22] and [27] proposes the correlation Eq. (23) in the case of packed wire screens used in Stirling engines.

$$Nu=\frac{h_p D_h}{k_g}=pRe_h^q,\quad p=0.33,\quad q=0.67\tag{23}$$

h_{int} is usually chosen equal to h_p.

Then, Eqs. (19) to (21) are transformed to obtain a non-dimensional system of equations that can be solved by using a Laplace transform on the time variable. The basic equations and the solving process are exposed in Appendix A. It is necessary to solve a third order differential equation and to determine its roots and the usual constants. This procedure is a fastidious mathematical task actually, but finally the Laplace transform of the temperature can be expressed in the following form:

$$\begin{aligned}\hat{\theta}_t&=C_1e^{r_1\chi}+C_2e^{r_2\chi}+C_3e^{r_3\chi}\\\hat{\theta}_g&=\left(ar_1^2+c\right)C_1e^{r_1\chi}+\left(ar_2^2+c\right)C_2e^{r_2\chi}+\left(ar_3^2+c\right)C_3e^{r_3\chi}\\\hat{\theta}_s&=\left(ar_1^2+c\right)C_1ke^{r_1\chi}+\left(ar_2^2+c\right)C_2ke^{r_2\chi}+\left(ar_3^2+c\right)C_3ke^{r_3\chi}\end{aligned}\tag{24}$$

The constants C_1, C_2, C_3 are calculated by verifying the specific boundaries conditions Eqs. (25)–(27); their expressions are reported in Appendix A. r_1, r_2 and r_3, are the roots of the characteristic equation associated to differential Eq. (A.15) of Appendix A. Because their literal expressions are quite complex, they are not reported here: in fact they are calculated during the solving procedure by the mathematics software "*MATHEMATICA*" automatically.

$$x=0\quad\overline{T}_{g,\text{re}}(x=0,t)=T_{\text{ge}}(t)\quad\text{and}\quad\frac{\partial\overline{T}_s}{\partial x}=\frac{\partial\overline{T}_{w,\text{re}}}{\partial x}=0\tag{25}$$

$$x=l_{\text{re}}\quad\frac{\partial\overline{T}_s}{\partial x}=\frac{\partial\overline{T}_{w,\text{re}}}{\partial x}=0\tag{26}$$

$$t=0\quad\overline{T}_{g,\text{re}}(x)=\overline{T}_{w,\text{re}}(x)=\overline{T}_s(x)=T_a\tag{27}$$

Knowing the solutions Eq. (24), the original expressions of the temperatures are extracted by using a numerical method for achieving Laplace transform inversion: Stehfest algorithm (see Appendix B).

In fact, all these results have been obtained in the case of regenerators of cylindrical geometry. Therefore, they cannot be applied to the considered micro regenerator of rectangular

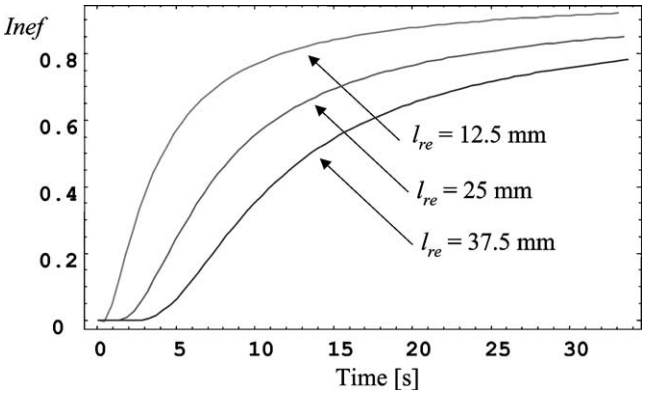

Fig. 13. Influence of the regenerator length on its theoretical inefficiency.

geometry directly. However, this difficulty can be solved quite easily by introducing new expressions of the specific areas from Eq. (22):

$$\sigma_1 = \frac{2}{w_f}, \qquad \sigma_2 = \sigma_{\text{ext}} = \frac{1}{e_{\text{gl}}} \tag{28}$$

With this theoretical model, the thermal responses to a temperature step of the gas at the regenerator inlet can be easily studied (considering constant pressure and mass flow rate). Moreover, the thermal response to an arbitrary inlet gas temperature can be also calculated by using the convolution product:

$$\hat{\theta}(\chi,\tau) = \hat{\theta}_{g,\text{inlet}}(0,\tau) * \hat{\theta}_{\text{imp}}(\chi,\tau) \tag{29}$$

The first term is the Laplace transform of the inlet fluid temperature, while the second one represents the impulse response of the exchanger to a delta Dirac function of the fluid inlet temperature.

Thus, in the case of a step excitation, the regenerator inefficiency can be defined with Eq. (30):

$$\begin{aligned} \mathit{Inef}(t) &= 1 - \frac{\int_0^t (T_{g,\text{lre}}(u) - T_{g,\text{inlet}})\,\mathrm{d}u}{T_a - T_{g,\text{inlet}}} \\ &= \frac{\int_0^t (T_{g,\text{lre}}(u) - T_a)\,\mathrm{d}u}{T_{g,\text{inlet}} - T_a} \end{aligned} \tag{30}$$

It is defined as the ratio of the heat quantity exchanged between the fluid and the material divided by the maximal heat quantity that could be exchanged if fluid exit temperatures was identical to the initial temperature (supposed equal to that of the surrounding).

Fig. 13 shows the numerical results of the inefficiency for different lengths l_{re} of the micro regenerator considering the inlet temperature, mass flow rate, and pressure as constant values. In all cases, the inefficiency reaches an excessive value after a time delay increasing with respect to the regenerator length. In fact, these curves indicate that the frequency is an important parameter for designing the regenerator geometry. Moreover, these curves are deduced from the device response to a step function. In reality, with a periodic regime, the regenerator may operate in worth conditions so that its inefficacy is undervalued. Therefore, a length of 25 mm respects condition of Eq. (10) and seems to be a good compromise for guaranteeing optimal thermal effects while minimizing pressure drop phenomena.

4.2.2. Thermal modeling of the compact micro heat exchangers

The structure and the function of the heat exchangers are very similar to those of the regenerator (compactness, single fluid), hence a few adaptations allow to apply the previous theoretical analysis to heat exchangers for evaluating their thermal transitory response with a good accuracy. In this idea, the equations system (15) is modified as following (Φ^* represents an additional source term to represent the heat production of an electronic component that may be placed on the cold exchanger: null in this study).

$$\left(\frac{\partial \overline{T}_g}{\partial t} + \overline{U}\frac{\partial \overline{T}_g}{\partial x}\right) = \frac{\sigma_1 h_{\text{int}}}{\rho_g c_g}\left(\overline{T}_w - \overline{T}_g\right) \tag{31}$$

$$\begin{aligned} \frac{\partial \overline{T}_w}{\partial t} &= \Phi^* + \frac{\sigma_{\text{ext}} h_{\text{ext}}}{\rho_w c_w}\left(T_a - \overline{T}_w\right) \\ &\quad + \frac{\sigma_2 h_{\text{int}}}{\rho_w c_w}\left(\overline{T}_g - \overline{T}_w\right) + \frac{k_w}{\rho_w c_w}\frac{\partial^2 \overline{T}_w}{\partial x^2} \end{aligned} \tag{32}$$

Only the equation for the gas Eq. (31) and for the envelope Eq. (32) are required; nevertheless, a weighting factor η_s related to the internal finned structure is introduced (see Appendix C) and new specific areas and coefficients of Eq. (22) are defined:

$$\begin{aligned} &\sigma_1 = \frac{2N\lambda}{S_{\text{pass}}}\eta_s, \qquad \sigma_2 = \frac{2N\lambda}{S_w} \\ &\sigma_{\text{ext}} = \frac{N\lambda}{S_w}, \qquad \Phi^* = \frac{N\lambda\Phi}{S_w \rho_w c_w} \\ &S_{\text{pass}} = N(\lambda - e_f)w_f \\ &S_w = N(\lambda e_{\text{gl}} + \lambda e_{\text{Si}} + w_f e_f) \end{aligned} \tag{33}$$

In Eq. (32), the solid phase is calculated by using the average thermo-physical properties estimated as following:

$$\begin{aligned} a_w^* &= \frac{k_w}{\rho_w c_w} \\ \rho_w c_w &= \frac{\rho_f c_f e_f w_f + \rho_{\text{gl}} c_{\text{gl}} e_{\text{gl}}\lambda + \rho_{\text{Si}} c_{\text{Si}} e_{\text{Si}}\lambda}{e_f w_f + e_{\text{gl}}\lambda + e_{\text{Si}}\lambda} \\ k_w &= \frac{k_f e_f w_f + k_{\text{gl}} e_{\text{gl}}\lambda + k_{\text{Si}} e_{\text{Si}}\lambda}{e_f w_f + e_{\text{gl}}\lambda + e_{\text{Si}}\lambda} \end{aligned} \tag{34}$$

The Petukov correlation [28], established for the entrance region of conduits of oblong section, is used for estimating the internal coefficient h_{int} (static flow).

$$\begin{aligned} Nu = \frac{h_{\text{int}} D_h}{k_g} &= 4.36 + 1.31\left(Re_h P_r \frac{D_h}{x}\right)^{0.33} \\ &\quad \times \exp\left(-13\sqrt{\frac{x}{Re_h P_r D_h}}\right) \end{aligned} \tag{35}$$

for

$$\frac{x}{Re_h P_r D_h} > 0.001$$

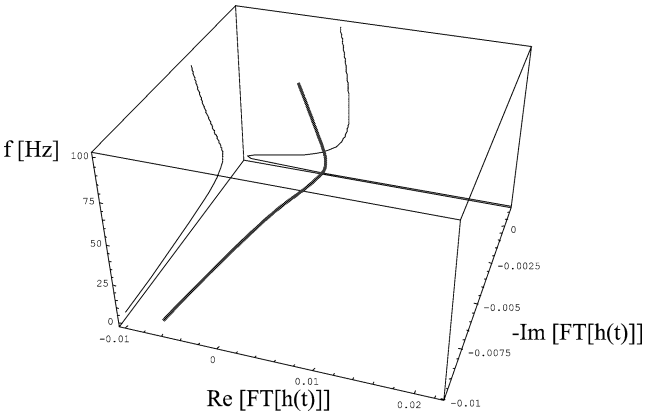

Fig. 14. Theoretical impulse response, complex transfer function of the heat exchanger (3.36 mm long—velocity of 1.5 m·s^{-1} and inflating pressure of 1.2 MPa).

The calculus of Appendix A are applicable to a micro-scale exchanger by using the following particular parameters:

$$\varepsilon = 1, \qquad B = B_0 = 0 \tag{36}$$

The study of the Fourier transform of the impulse response $h(t)$ of an exchanger seems a good way to represent its transient behavior because it provides a representation of the transfer function of the exchanger. One can easily obtain this Fourier transform from the calculus of the Laplace transform of the theoretical modeling by substituting the term $2\pi f.j$ to the Laplace parameter, remarking the non-dimensional temperature is null in the range $]-\infty, 0[$. Fig. 14 gives a 3D representation of the transfer function of the heat exchanger. It is observed that its amplitude decreases very quickly with respect to the frequency. Its imaginary part remains always positive and also decreases very quickly when the frequency increases. The real part varies differently: indeed, it strongly decreases and passes by a minimal value slightly negative. This indicates that complex phenomena are likely to introduce significant delays according to the operating frequency. However, these effects are significant only at low frequencies which are not used for this cooler type generally. This is why the analysis of the complex transfer function modulus is sufficient. Fig. 15 shows the evolution of this quantity depending on the frequency for compact micro exchangers of various lengths. As well as the modulus of the transfer function decreases all the more quickly, the exchanger length is increased. In fact, if the transfer function remained equal to its initial value of 1, that would indicate that the temperature at the outlet is identical to that of the inlet: so no heat transfer would occur in the exchanger and it would be inefficient completely. Thus Fig. 15 naturally shows that the heat exchangers may be as long as possible. However it is necessary to preserve an exchanger which dimensions are compatible with reasonable pressure drop and with a convenient volume (in fact this one constitutes a dead volume for the whole refrigerator and diminishes its performances). These remarks show that

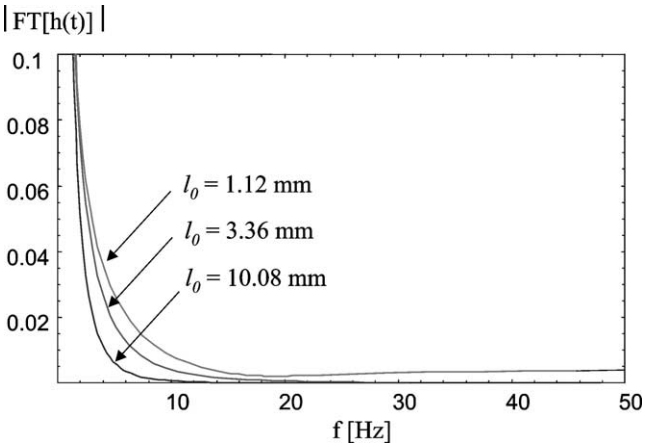

Fig. 15. Theoretical influence of the heat exchangers length on the complex transfer function modulus, i.e., impulse response (velocity of 1.5 m·s^{-1} and inflating pressure of 1.2 MPa).

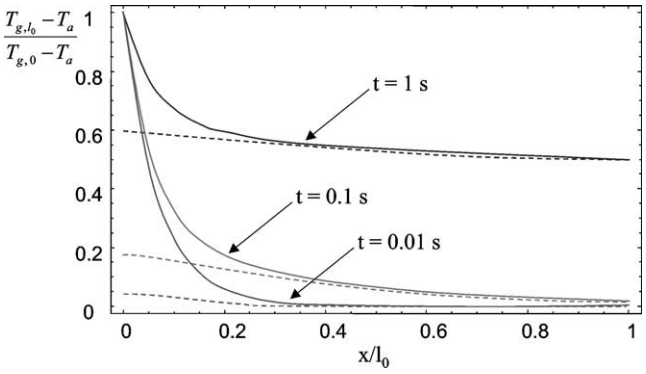

Fig. 16. Walls (dashed line) and gas theoretical temperature distributions along a heat exchanger, step response (3.36 mm long—velocity of 1.5 m·s^{-1} and inflating pressure of 1.2 MPa).

a 3.36 mm length seems to be a good compromise, taking into account the use of a minimal frequency of 30 Hz.

Another way to check the exchangers performances consists in examining the thermal response, not to an impulse function but to a step function. It is supposed that the initial temperature of the exchanger is uniform and equal to the surrounding temperature T_a. At the origin of time, a step function of temperature $T_{g,0}$ flows through the exchanger ("single blow" method). The temperature profiles in the gas and in silicon walls are considered. They are reported on Fig. 16 for various instants in the case of an exchanger of 3.36 mm length. These results show that whatever the time, the gas temperature joins that of silicon at a distance corresponding to 40% of the exchanger length approximately. Taking into account the calculus assumptions, these results makes it possible to validate the choice of a 3.36 mm length exchanger, the additional pressure drops due to the excess of length remaining acceptable. Nevertheless the condition of Eq. (10) is poorly satisfied, the ratio being not very superior to the required value.

5. Experiments on the module: Thermal performances

The prototype presented on Fig. 5 has been instrumented by a set of temperature and pressure micro-sensors. A 350 ohm electric resistance in film, stuck on the carved wall of the cold zone, allows to simulate the thermal load. The temperatures are measured at various locations by means of micro-thermocouples (K type) of 75 μm diameter. The pressure sensors are piezoelectric miniaturized sensors of large cut off frequency. They are placed on the capillaries connections at the inlet and the outlet of the passive module. A compressor and a sufficiently large reservoir are linked to these extremities, respectively. A specific facility with vacuum pump and helium taps is used to fill the device. The inflation is completed at a maximal pressure of 1.2 MPa.

The thermal performances are evaluated in dynamic regime. The operating frequency is adjustable up to a maximal value of 50 Hz. During experiments, the best cooling performances were obtained when both the frequency and the inflating pressure were maximum (1.2 MPa and 50 Hz), confirming the theoretical predictions. The experimental thermal results are summarized on Fig. 17: a global temperature reduction of about 10 to 12 °C is observed at the cold zone; simultaneously a heating about 5 to 7 °C appears at the external walls of the first heat exchanger (after the compressor) while the last exchanger remains at a constant temperature slightly greater than T_a. These results permit to evaluate the net cooling power of the micro DIOPTR, thanks to the measured electrical power supplied to the resistance coated at the cold zone: Fig. 18 shows the evolution of this parameter as a function of the measured cold zone temperature. A net cooling power about 50 mW is obtained at the ambient temperature. The performances of this first prototype remain relatively modest because heat losses mentioned in Eq. (5) are still too much important.

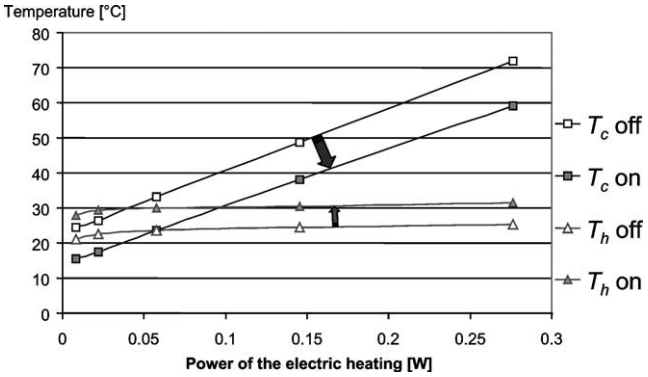

Fig. 17. Temperature evolutions on the cold and warm zones with (on) and without (off) compressor, inflating pressure 1.2 MPa, frequency 50 Hz.

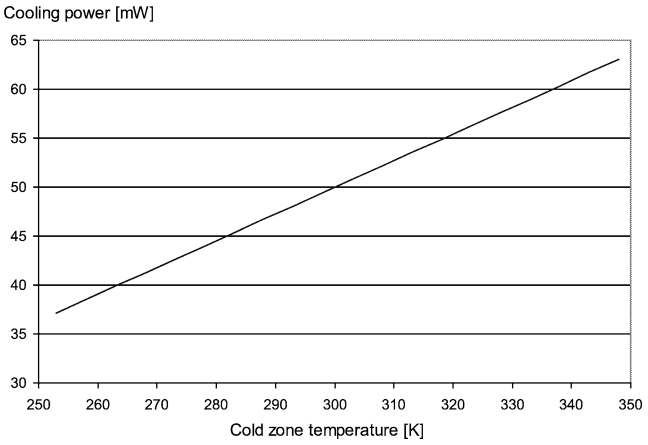

Fig. 18. Net cooling power of the micro DIOPTR versus cold zone temperature, inflating pressure 1.2 MPa, frequency 50 Hz.

6. Conclusions

The work presented in this paper has demonstrated the DIOPTR principle to be utterly compatible with the development of a micro refrigerator dedicated to the cooling of electronic systems. The micro-fabrication technologies usually used in microelectronics are entirely compatible with the small scale of such a cooler. However, the use of classical materials (silicon and glass) imposed by these techniques leads to important thermal losses because of their high thermal specific conductivity. As a result, the net cooling power supplied by the first prototype is relatively weak and the temperature decrease of the cold zone remains quite modest. Nevertheless, in order to improve the cooling power, the authors intend to modify the geometry of the passive module: a first solution consists in using a U shaped tube to put the two hot exchangers at the same side, and the cold zone at the opposite side; thus thermal gradients are divided by 2 if the global dimensions are conserved. This also allows to increase the pulse tube volume, minimizing the shuttle thermal effects. An additional solution is to reduce the glass slabs thickness or to find another material that could be gathered with silicon.

Besides, this work underlines the lack of knowledge concerning the field of research dedicated to periodic flows with thermal transfers in micro systems. Most laboratories designing such devices use classical physical formulations established for static regimes and not entirely applicable to the considered problem. The original approach proposed by the authors consists in studying the transient thermal response of a system by calculating its transfer function (Laplace and Fourier transforms). Thus, the micro-regenerator and micro-exchangers design is achieved by considering the response to an impulse or/and a step function (inlet temperature history). In fact the study is carried “a posteriori” in static regime with constant values of fluid velocity and pressures; these values are maximal values obtained in a first time with the complete modeling of the cooler [15,18] and considering ideal exchangers. The micro exchangers design, functioning in real conditions, and its combination with the global DIOPTR model remains a far objective actually. Therefore, the experimental way still constitutes an essential step for adjusting the different coefficients (pressure drop, Nusselt number . . .)

used in theoretical models. Moreover experiments are indispensable to get information on pulsed flows and periodic heat transfers, especially at small scale. The authors intend to complete the experimental apparatus: others physical quantities like velocity or mass flow rate could be investigated by means of optical techniques [29] (PIV, LDV). In order to obtain information on the physical quantities amplitudes but also on their phases, additional internal measurements are planned. For example, the dynamic, temperature fluctuations could be investigated by means of micro-thermocouples [28] or thin film thermocouples [29] deposited on the internal wall of the device.

As discussed in the introduction the constant improvements of both power and compactness in electronics requires more and more efficient cooling methods: in the near future a density of heat dissipation about a few hundred $\mathrm{W\cdot cm^{-2}}$ will become current. Most usual cooling systems (radiators, ventilation, heat pipes, water circulation in microchannels) are relevant while the required functioning temperature is not lower than the ambient temperature actually. The DIOPTR does not present this limitation because it is an active cooler obviously. Specialists predict that the cooling of electronic processor to a cryogenic temperature (≈ 80 K) would permit to modify its functioning frequency (so its power) by a factor $\times 4$. In addition, many detectors (infrared, gamma ray, ultra violet) must operate at similar temperature levels to avoid noise due to thermal agitation, many biomedical applications require a cooling process and cryotherapy is at the beginning of its development. Therefore, it is essential to continue the researches on micro coolers and especially on micro DIOPTR. The authors think the technology presented in this paper, combining the fabrication processes of microelectronics and the design of a thermodynamic machine is of great interest and allows to expect many improvements in the near future. In particular, this technology could also be applied to the design of the compressor and moreover the electronic component to be cold could be integrated in the silicon matrix, thus both the electronic and the cooling functions could be grouped in a single "electro-cooled-component".

Acknowledgements

This work was partly supported by Thales Cryogenie, 4 rue Marcel Doret, 31 701 Blagnac Cedex France. The authors thank Jacques De Lallée and Véronique Pugliese.

Appendix A

The non-dimensional variables definitions are:

$$\chi = x/l_{\mathrm{re}}, \qquad \tau = t/R_c$$
$$\theta_\zeta = \frac{\overline{T}_\varsigma(\chi,\tau) - T_a}{T_{\varsigma e0} - T_a} \quad (\zeta = g, s, w) \tag{A.1}$$

The characteristic time for the material heating with a given mass flow rate of fluid is defined by:

$$R_c = \frac{l_{\mathrm{re}}}{\overline{\overline{U}}} \frac{\rho_s c_s (1-\varepsilon) + \rho_w c_w S_w/S_{\mathrm{int}}}{\rho_g c_g} \tag{A.2}$$

The following practical parameters are also introduced:

$$B = R_c \frac{h\sigma_p}{(1-\varepsilon)\rho_s c_s}, \qquad B_0 = \frac{h\sigma_p}{\rho_g c_g} \frac{l_{\mathrm{re}}}{\overline{\overline{U}}}$$
$$B_1 = \frac{l_{\mathrm{re}}}{\overline{\overline{U}}} \frac{\varepsilon\sigma_1 h'}{\rho_g c_g}, \qquad B_2 = \frac{\sigma_2 h'}{\rho_w c_w} R_c \tag{A.3}$$
$$B_e = \frac{\sigma_e h_e}{\rho_w c_w} R_c$$

System of equations to be solved from (13)–(15):

$$\frac{L\varepsilon}{\overline{U} R_c} \frac{\partial\theta_g}{\partial\tau} + \frac{\partial\theta_g}{\partial\chi} + B_0(\theta_g - \theta_s) + B_1(\theta_g - \theta_w) = 0$$
$$\frac{\partial\theta_s}{\partial\tau} - B(\theta_g - \theta_s) = 0 \tag{A.4}$$
$$\frac{\partial\theta_w}{\partial\tau} + B_e\theta_w - B_2(\theta_g - \theta_w) = \frac{a_w^* R_c}{l_{\mathrm{re}}^2} \frac{\partial^2\theta_w}{\partial\chi^2}$$

The boundary (spatial and temporal) conditions are:

$$\chi = 0, \quad \theta_g = F_g(\tau), \qquad \left.\frac{\partial\theta_s}{\partial\chi}\right|_0 = \left.\frac{\partial\theta_w}{\partial\chi}\right|_0 = 0$$
$$\chi = 1, \quad \left.\frac{\partial\theta_s}{\partial\chi}\right|_1 = \left.\frac{\partial\theta_w}{\partial\chi}\right|_1 = 0 \tag{A.5}$$
$$\tau = 0, \quad \theta_g(\chi) = \theta_s(\chi) = \theta_w(\chi) = 0$$

Tacking the Laplace transform of the systems (A.4) and (A.5) (variable: time):

$$L\big[\theta(\chi,\tau)\big] = \hat{\theta}(\chi, p)$$
$$\frac{l_{\mathrm{re}}\varepsilon}{\overline{\overline{U}} R_c} p\hat{\theta}_g + \frac{\partial\hat{\theta}_g}{\partial\chi} + B_0\big(\hat{\theta}_g - \hat{\theta}_s\big) + B_1\big(\hat{\theta}_g - \hat{\theta}_w\big) = 0$$
$$p\hat{\theta}_s - B\big(\hat{\theta}_g - \hat{\theta}_s\big) = 0 \tag{A.6}$$
$$p\hat{\theta}_w + B_e\hat{\theta}_w - B_2\big(\hat{\theta}_g - \hat{\theta}_w\big) = \frac{a_w^* R_c}{l_{\mathrm{re}}^2} \frac{\partial^2\hat{\theta}_w}{\partial\chi^2}$$

$$\chi = 0, \quad \hat{\theta}_g(0, p) = \widehat{F}(p), \quad \left.\frac{\partial\hat{\theta}_s}{\partial\chi}\right|_0 = \left.\frac{\partial\hat{\theta}_w}{\partial\chi}\right|_0 = 0 \tag{A.7}$$

$\widehat{F}(p) = 1$ impulse function, $\widehat{F}(p) = 1/p$ step function

$$\chi = 1, \quad \left.\frac{\partial\hat{\theta}_s}{\partial\chi}\right|_1 = \left.\frac{\partial\hat{\theta}_w}{\partial\chi}\right|_1 = 0$$

for the variables of (A.6), one obtains:

$$\hat{\theta}_s = \frac{B}{p+B}\hat{\theta}_g$$
$$\hat{\theta}_g = -\frac{a_w^* R_c}{B_2 l_{\mathrm{re}}^2} \frac{\partial^2\hat{\theta}_w}{\partial\chi^2} + \frac{(p + B_e + B_2)}{B_2}\hat{\theta}_w \tag{A.8}$$

and substituting this relation in the first equation of (A.6), one finds a third order differential equation representing the Laplace transform of the wall temperature:

$$-\frac{a_w^* R_c}{B_2 l_{\mathrm{re}}^2}\frac{\partial^3\hat{\theta}_w}{\partial\chi^3}-\frac{a_w^* R_c}{B_2 l_{\mathrm{re}}^2}\left(\frac{l_{\mathrm{re}}\varepsilon}{R_c\overline{U}}p+B_1+\frac{B_0 p}{p+B}\right)\frac{\partial^2\hat{\theta}_w}{\partial\chi^2}+\frac{(p+B_e+B_2)}{B_2}\frac{\partial\hat{\theta}_w}{\partial\chi}+\left(\left(\frac{l_{\mathrm{re}}\varepsilon}{R_c\overline{U}}p+B_1+\frac{B_0 p}{p+B}\right)\times\frac{(p+B_e+B_2)}{B_2}-B_1\right)\hat{\theta}_w=0 \tag{A.9}$$

To simplify the previous form, new parameters are adopted:

$$a=-\frac{a_w^* R_c}{B_2 l_{\mathrm{re}}^2} \tag{A.10}$$

$$b(p)=-\frac{a_w^* R_c}{B_2 l_{\mathrm{re}}^2}\left(\frac{l_{\mathrm{re}}\varepsilon}{R_c\overline{U}}p+B_1+\frac{B_0 p}{p+B}\right) \tag{A.11}$$

$$c(p)=\frac{(p+B_e+B_2)}{B_2} \tag{A.12}$$

$$d(p)=\left(\left(\frac{l_{\mathrm{re}}\varepsilon}{R_c\overline{U}}p+B_1+\frac{B_0 p}{p+B}\right)\times\frac{(p+B_e+B_2)}{B_2}-B_1\right) \tag{A.13}$$

$$k(p)=\frac{B}{B+p} \tag{A.14}$$

Thus the third order equation (A.9) becomes:

$$a(p)\frac{\partial^3\hat{\theta}_w}{\partial\chi^3}+b(p)\frac{\partial^2\hat{\theta}_w}{\partial\chi^2}+c(p)\frac{\partial\hat{\theta}_w}{\partial\chi}+d(p)\hat{\theta}_w=0 \tag{A.15}$$

and the other Eqs. (A.8) lead to:

$$\hat{\theta}_g=a(p)\frac{\partial^2\hat{\theta}_w}{\partial\chi^2}+c(p)\hat{\theta}_w=0 \tag{A.16}$$

$$\hat{\theta}_s=k(p)\hat{\theta}_g=0 \tag{A.17}$$

The solutions of (A.15) is obtained by evaluating the roots r_1, r_2, r_3 of the characteristic equation; this is achieved by a calculus procedure implemented in the software *MATHEMATICA*:

$$\begin{aligned}\hat{\theta}_w&=C_1e^{r_1\chi}+C_2e^{r_2\chi}+C_3e^{r_3\chi}\\ \hat{\theta}_g&=\left(ar_1^2+c\right)C_1e^{r_1\chi}+\left(ar_2^2+c\right)C_2e^{r_2\chi}\\ &\quad+\left(ar_3^2+c\right)C_3e^{r_3\chi}\\ \hat{\theta}_s&=\left(ar_1^2+c\right)C_1ke^{r_1\chi}+\left(ar_2^2+c\right)C_2ke^{r_2\chi}\\ &\quad+\left(ar_3^2+c\right)C_3ke^{r_3\chi}\end{aligned} \tag{A.18}$$

With the boundaries conditions, the constants can be extracted:

$$\begin{aligned}C_1&=r_2r_3\left(e^{r_2}-e^{r_3}\right)\widehat{F_g}(p)\\ &\quad\times\left[r_2r_3\left(ar_1^2+c\right)\left(e^{r_2}-e^{r_3}\right)\right.\\ &\quad-r_1r_3\left(ar_2^2+c\right)\left(e^{r_1}-e^{r_3}\right)\\ &\quad\left.-r_1r_2\left(ar_3^2+c\right)\left(e^{r_2}-e^{r_1}\right)\right]^{-1}\end{aligned} \tag{A.19}$$

$$C_2=-\frac{r_1}{r_2}C_1\frac{e^{r_1}-e^{r_3}}{e^{r_2}-e^{r_3}} \tag{A.20}$$

$$C_3=-\frac{r_1}{r_3}C_1\frac{e^{r_2}-e^{r_1}}{e^{r_2}-e^{r_3}} \tag{A.21}$$

Appendix B

The Stehfest algorithm for the Laplace transform inversion is:

$$\theta(\tau_m)=\frac{\ln 2}{\tau_m}\sum_{i=1}^{10}v(i,n).\bar{\theta}\left(\frac{i\ln 2}{\tau_m}\right) \tag{B.1}$$

where Stehfest's vector is given by:

$$v(i,n_{\mathrm{pair}})=(-1)^{n_{\mathrm{pair}}/2+i}\sum_{\mathrm{Ent}[i+1/2]}^{\mathrm{Min}[i,n_{\mathrm{pair}}/2]}k^{n_{\mathrm{pair}}/2}\times\frac{(2k)!}{(n_{\mathrm{pair}}/2-k)!k!(k-1)!(i-k)!(2k-i)!} \tag{B.2}$$

n_{pair} is an even number equal to 10 for reaching a convenient precision.

Appendix C

For an embedded fin of temperatures T_{ph} and T_{pb}, respectively, for the bottom and top extremities and bathed by a fluid of constant temperature T_g, the temperature evolution along the fin is given by (see Fig. 12):

$$T(z)-T_g=(T_{ph}-T_g)\frac{e^{-mz}-e^{mz}}{e^{-mw_f}-e^{mw_f}}+(T_{pb}-T_g)\frac{e^{-m(w_f-z)}-e^{m(w_f-z)}}{e^{-mw_f}-e^{mw_f}} \tag{C.1}$$

with

$$m^2=\frac{h_i p}{k_a S},\qquad S=e_f l_0,\qquad p=2(e_f+l_0) \tag{C.2}$$

Several geometrical parameters are also used:

$A=Ne_f l_0$	area with fins
$B=(1+N)(\lambda-e_f)l_0$	area without fins
$\Sigma_a=w_f(e_f+l_0)$	1/2 external area of one fin
$\Sigma=Nw_f(e_f+l_0)$	1/2 external area of fins

The efficiency of a fin is:

$$\eta_a=-\frac{k_a S(\partial T/\partial z|_{z=0}-\partial T/\partial z|_{x=w_f})}{h_i\Sigma_a(T|_{z=0}+T|_{z=w_l}-2T_g)}=\frac{p}{m\Sigma_a}\frac{2-(e^{mw_l}+e^{-mw_l})}{e^{-mw_l}-e^{mw_l}} \tag{C.3}$$

The thermal flux exchanged with the fluid is:

$$\dot{Q}=h_i(B+\eta_a\Sigma)(T_{ph}+T_{pb}-2T_g) \tag{C.4}$$

and the heat flow between two plates is:

$$\dot{Q}^* = h_i(A+B)(T_{ph}+T_{pb}-2T_g) \quad \text{(C.5)}$$

The weight factor of the finned structure is defined by:

$$\eta_s = \frac{\dot{Q}}{\dot{Q}^*} = \frac{B}{A+B} + \eta_a \frac{\Sigma}{A+B} \quad \text{(C.6)}$$

References

[1] C.Y. Zhao, T.J. Lu, Analysis of microchannel heat sinks for electronics cooling, Internat. J. Heat Mass Transfer 45 (2002) 4857–4869.

[2] M. Groll, M. Schneider, V. Sartre, M. Chaker Zaghdoudi, M. Lallemand, Thermal control of electronic equipment by heat pipes, Rev. Gén. Therm. 37 (1998) 323–352.

[3] D.T. Kuo, A.S. Loc, S.W.K. Yuan, A.L. Johnson, Design of a 0.5 watt dual use long-life low-cost pulse tube cooler, Adv. Cryogenic Engrg. 43 (1998) 2039–2046.

[4] T. Nast, P. Champagne, V. Kotsubo, Development of a low-cost unlimited-life pulse-tube cryocooler for commercial applications, Adv. Cryogenic Engrg. 43 (1998) 2047–2053.

[5] C. Dolabdjian, S. Saez, D. Bloyet, M. David, J.C. Marechal, Progress towards a hand portable pulse tube refrigerator for high TC dc SQUID operation, Appl. Superconductivity 6 (7–9) (1998) 459–464.

[6] J. Liang, Y. Zhou, W. Zhu, W. Sun, J. Yang, S. Li, Study on miniature pulse tube cryocooler for space application, Cryogenics 40 (2000) 229–233.

[7] C.K. Chan, P. Clancy, J. Godden, Pulse tube cooler for fligth hyperspectral imaging, Cryogenics 39 (2000) 1007–1014.

[8] E. Tward, C.K. Chan, C. Jaco, J. Chapsy, P. Clansy, Miniature space pulse tube cryocoolers, Cryogenics 39 (2000) 717–720.

[9] E.I. Mikulin, A.A. Tarasov, M.P. Shkrebyonock, Low temperature expansion pulse tube, Adv. Cryogenic Engrg. 29 (1984) 629–637.

[10] B. Zhou, P. Wu, S. Hu, G. Chen, Experimental results of the internal process of a double inlet pulse tube refrigeratior, Cryogenics 32 (1992) 24–27.

[11] C. Wang, P. Wu, Z. Chen, Modified orifice pulse tube refrigerator without a reservoir, Cryogenics 34 (1) (1994) 31–36.

[12] C.M. Gao, Y.L. He, Z.Q. Chen, Study on a pulse tube cryocooler using gas mixture as its working fluid, Cryogenics 40 (2000) 475–480.

[13] Sang Ho Baek, Eun Soo Jeong, Sangkwon Jeong, Two-dimensional model for tapered pulse tubes. Part 1: Theoretical modeling and net enthalpy flow, Cryogenics 40 (2000) 379–385.

[14] J. Yuan, J.M. Pfotenhauer, Thermodynamic analysis of active valve pulse tube refrigerators, Cryogenics 39 (1999) 283–292.

[15] Y. Bailly, P. Nika, M. De Labachelerie, J.C. Jeannot, J. De Lallée, Vers la miniaturisation d'une machine frigorifique de type Tube à Gaz Pulsé, in: Congrès Français de Thermique, Nantes 29–31 mai, 2001.

[16] G. Popescu, V. Radcenco, E. Gargalian, P.R. Bola, A critical review of pulse tube cryogenerator research, Internat. J. Refrig. 24 (2001) 230–237.

[17] R. Radebaugh, A review of pulse tube refrigeration, Adv. Cryogenic Engrg. 35 (1990) 1191–1205.

[18] P. Nika, Modélisations et méthodes expérimentales pour l'étude des réfrigérateurs de type Stirling et tube à gaz pulsé : application à la miniaturisation des refroidisseurs, Ph.D. Thesis, University of Franche-Comté, France, 2002.

[19] W.M. Rohsenow, J.P. Hartnett, Y.I. Cho, Handbook of Heat Transfer, 3rd Edition, McGraw-Hill, New York.

[20] G.W. Swift, Thermoacoustics: A unifying perspective for some engines and refrigerators, Fifth draft, LA UR 99 895, May 2001.

[21] C. Aubert, Ecoulements compressibles de gaz dans les microcanaux: effets de raréfaction, effets instationnaires, Thèse de l'Univérsité Paul Sabatier, n° 3349, 1999.

[22] S. Reza, Charles J. Call, State of the art in micro and meso scale heat exchangers, in: AES, Vol. 39, Proc. of the ASME 53-61.

[23] H. Miyabe, S. Takahashi, K. Hamaguchi, An approach to the design of Stirling engine regenerator matrix using packs of wire gauzes, in: IEEE 17th IECEC, 1982, pp. 1839–1844.

[24] M. Tanaka, I. Yamashita, F. Chisaka, Flow and heat transfert characteristics of the Stirling engine regenerator in an oscillating flow, JSME Internat. J. Ser. (2) 33 (2) (1990) 283–289.

[25] E. Poncet, P. Nika, D. Bereiziat, Technique de caractérisation d'un mini-régénérateur thermique pour mini-refroidisseur Stirling ou tube à gaz pulsé, Mech. Ind. (2001) 455–464.

[26] B. Thomas, D. Pittman, Update on the evaluation of different correlations for the flow friction factor and the heat transfert of Stirling engine regenerators, AIAA-2000-2812, 76–84.

[27] J.P. Prenel, Optical systems for fluids mechanics investigations, Invited paper, in: Proceedings of the Second International Conference on Optical Design and Fabrication, Tokyo, November, 2000, pp. 129–132.

[28] Y. Bailly, F. Lanzetta, L. Thiery, L. Girardot, Dynamic calibration for micronic and submicronic thermoelectric sensors, in: Eurotherm Seminar N°57, Microscale Heat Transfer, Poitiers, July 8–10, 1998.

[29] B. Serio, P. Nika, J.P. Prenel, Static and dynamic calibration of thin-film thermocouples by means of a laser modulation technique, Rev. Sci. Instruments 71 (2000) 4306–4313.